Oncogene
https://doi.org/10.1038/s41388-018-0643-z

ARTICLE

Genome-wide screening identifies oncofetal lncRNA Ptn-dt promoting the proliferation of hepatocellular carcinoma cells by regulating the Ptn receptor

Jin-Feng Huang[1,2] · Hong-Yue Jiang[3] · Hui Cai[4] · Yan Liu[1] · Yi-Qing Zhu[1] · Sha-Sha Lin[5] · Ting-Ting Hu[5] · Tian-Tian Wang[1,2] · Wen-Jun Yang[1] · Bang Xiao[1] · Shu-Han Sun[1,2] · Li-Ye Ma[4] · Hui-Rong Yin[5] · Fang Wang[1,2]

Received: 3 June 2018 / Revised: 4 October 2018 / Accepted: 23 November 2018

Abstract

Oncofetal genes are genes that express abundantly in both fetal and tumor tissues yet downregulated or undetected in adult tissues, and can be used as tumor markers for cancer diagnosis and treatment. Meanwhile, long noncoding RNAs (lncRNAs) are known to play crucial roles in the pathogenesis of hepatocellular carcinoma (HCC), including tumor growth, proliferation, metastasis, invasion, and recurrence. We performed a genome-wide screening using microarrays to detect the lncRNA expression profiles in fetal livers, adult livers, and liver cancer tissues from mice to identify oncofetal lncRNAs in HCC. From the microarray data analysis, we identified lncRNA Ptn-dt as a possible oncofetal gene. Both in vitro and in vivo experiments results confirmed that overexpression of Ptn-dt significantly promoted the proliferation of mouse HCC cells. RNA pulldown assay showed that Ptn-dt could interact with the HuR protein. Interestingly, miR-96 binds with HuR to maintain its stability as well. Overexpression of lncRNA Ptn-dt led to the downregulation of miR-96, which might be due to the interaction between Ptn-dt and HuR. Meanwhile, previous studies have reported that Ptn can promote tumor growth and vascular abnormalization via anaplastic lymphoma kinase (Alk) signaling. In our study, we found that overexpression of Ptn-dt could promote the expression of Alk through repressing miR-96 via interacting with HuR, thus enhancing the biologic function of Ptn. In summary, a new oncofetal lncRNA Ptn-dt is identified, and it can promote the proliferation of HCC cells by regulating the HuR/miR-96/Alk pathway and Ptn-Alk axis.

Introduction

Hepatocellular carcinoma (HCC) is one of the most common types of cancer worldwide and has a high morbidity and mortality rate [1]. Approximately 85% of HCC patients are from developing countries, particularly in regions with a high incidence of hepatitis B virus infection, such as Southeast Asia and sub-Saharan Africa [2]. The treatment strategies for patients with HCC include surgery, radiation, chemotherapy, liver transplantation, and targeted therapies. Despite improvements in the treatment protocols, the death rates are increasing for patients with HCC. The majority of studies showed that the 5-year survival rate was less than 5% [1]. Most HCC patients are diagnosed with

These authors contributed equally: Jin-Feng Huang, Hong-Yue Jiang, Hui Cai

Supplementary information The online version of this article (https://doi.org/10.1038/s41388-018-0643-z) contains supplementary material, which is available to authorized users.

✉ Li-Ye Ma
malydr@163.com

✉ Hui-Rong Yin
topyin@126.com

✉ Fang Wang
wfsjz@163.com

[1] Department of Medical Genetics, Second Military Medical University, 200433 Shanghai, China

[2] Department of Clinical Genetics, Changhai Hospital, Second Military Medical University, 200433 Shanghai, China

[3] Department of Gastroenterology, Zhongshan Hospital, Fudan University, 200032 Shanghai, China

[4] Department of General Surgery, Changhai Hospital, Second Military Medical University, 200433 Shanghai, China

[5] Center of Reproductive Medicine, Changhai Hospital, Second Military Medical University, 200433 Shanghai, China

advanced-stage cancer, and the prognosis is rather undesirable due to the late stage [3]. Therefore, strengthening our understanding of the molecular pathogenesis of HCC can promote the development of effective treatments and eventually improve the overall prognosis of HCC patients.

Increasing evidence suggests that tumor cells may grow and extend by co-opting the signaling pathways that are commonly active only during embryonic development. In liver cancer [4], lung cancer [5], colon cancer [6], and Wilms' tumor, gene expression patterns simulating the early developmental stages of the corresponding organ have been identified in the tumor profile. Some oncofetal molecules have entered the stage of clinical application as early diagnostic markers, therapeutic targets or prognostic indicators for various tumors [7, 8]. Many investigations have shown that hepatocarcinoma cells have many of the similar traits of early fetal hepatocytes, and that they re-employ certain fetal liver-specific transcription factors and signaling molecules, some of which are oncofetal molecules [9]. Some oncofetal proteins have been long employed as oncotargets for the diagnosis and treatment of HCC. For example, alpha fetoprotein, which was discovered in human fetal serum in 1956, is currently widely used as an early diagnostic marker and an indicator of the recurrence of HCC [10]. Spalt-Like Transcription Factor 4 (SALL4) is an oncofetal protein that is normally expressed in the human fetal liver and is silenced in the adult liver, and SALL4 can be used as a marker for a progenitor subclass of HCC with an aggressive phenotype [11].

Long noncoding RNAs (lncRNAs) are regulatory molecules that have been widely studied in recent years [12]. Many functional lncRNAs have been shown to play key roles in organ development and cancer pathogenesis [13]. Recently, it has been shown that some noncoding RNAs possess the features of oncofetal molecules and are involved in the regulation of carcinogenesis. LncRNA-H19, HOTAIR, and let-7 have been recognized as oncofetal RNAs and used as potential targets for tumor treatments [14–16]. Nevertheless, compared with the oncofetal proteins, only a few oncofetal RNAs have been identified and characterized in HCC. Therefore, a transcriptome-wide screening of oncofetal lncRNAs must be performed in HCC.

In our previous study, we examined the expression profiles of lncRNAs and mRNAs in the livers of fetal and adult mice by microarray and identified many fetal liver-specific lncRNAs, which were more highly expressed in fetal or neonatal mouse liver tissues than in adult mouse liver tissues. Further investigation showed that one of the lncRNAs, mPvt1, can promote cell proliferation, cell cycling, and the expression of stem cell-like properties in murine cells. Moreover, human lncRNA-hPVT1 was upregulated in HCC tissues, and patients with a higher expression of lncRNA-hPVT1 had a poor clinical prognosis. These results showed that lncRNA PVT1 was an oncofetal RNA [17].

To identify more oncofetal lncRNAs, we constructed a diethylinitrosamine (DEN)-induced mouse liver cancer model and examined the lncRNA expression profiles in fetal livers, adult livers, and liver cancer tissues from mice by microarray in this study. Many lncRNAs were identified as new oncofetal lncRNAs in mice and were highly expressed in both fetal liver and liver cancer tissues. Among these lncRNAs, we identified the lncRNA Pleiotrophin (Ptn) downstream transcript (termed lncRNA Ptn-dt) and found that Ptn-dt can promote the proliferation of mouse HCC cells. Interestingly, we found that Ptn-dt could interact with HuR which might influence the binding of HuR to miR-96; therefore, the stability of miR-96 was disturbed, and the expression of miR-96 was decreased, which subsequently weakened the effect of miR-96 on the post-transcriptional inhibition of anaplastic lymphoma kinase (Alk) protein, which is a downstream target of Ptn. Finally, we concluded that Ptn-dt promoted the proliferation of HCC cells by regulating the HuR/miR-96/Alk pathway and Ptn-Alk axis.

Results

Differential lncRNA expression profiles in fetal liver, adult liver, and liver cancer tissues from mice

To identify oncofetal transcripts that potentially affect the occurrence and development of HCC, we established a DEN-induced mouse liver cancer model to obtain experimental samples, which are referred to as liver cancer in the following narrative. Mouse models have identical genetic background, thus providing experimental materials with good consistency, comparing to the individual variances in human HCC tissues. The liver cancer tissues were subjected to hematoxylin−eosin staining (HE staining) and verified according to their cell morphology under a microscope (Fig. 1a). Then, we analyzed the expression profiles of lncRNAs and protein-coding RNAs in 17.5-day-old embryonic livers (group A, three independent replicate samples named A1, A2, and A3), 2-month-old adult male mouse livers (group B, three independent replicate samples named B1, B2, and B3) and 1-year-old male mouse liver cancer tissues (group C, three independent replicate samples named C1, C2, and C3) using a microarray analysis. These microarray data are accessible through Gene Expression Omnibus (GEO) with series accession number GSE99157. A differential expression profile of lncRNAs was obtained (fold-change> 2, P value < 0.05); the differential profile of group A vs. B had 8585 lncRNAs, that of C vs. B had 6349 lncRNAs, and

that of the intersection of the two groups (A vs. B and C vs. B) had 3334 lncRNAs. A differential expression profile of protein-coding RNAs was also obtained (fold-change > 2, P value < 0.05), in which the differential profile of A vs. B had 7655 protein-coding RNAs, that of C vs. B had 5166 protein-coding RNAs, and that of the intersection of the two groups (A vs. B and C vs. B) had 2971 protein-coding RNAs. The hierarchical clustering showed systematic variations in the transcript expression levels of the differentially expressed lncRNAs (Fig. 1b) and protein-coding RNAs (Supplementary Figure S1A) obtained from the intersection of the two groups (A vs. B and C vs. B). To our interest, there were 1070 oncofetal lncRNAs and 876 oncofetal protein-coding RNAs in the intersection of the two groups (A vs. B and C vs. B). Because biologically related gene groups can share the same patterns of change, we carried out the GO analysis and KEGG pathway analysis of the 876 oncofetal protein-coding RNAs to understand the behavior of these oncofetal lncRNAs (Supplementary Figure S1B). The KEGG pathway analysis (Fig. 1c) showed that these oncofetal protein-coding RNAs included many cell-cycle genes and DNA replication genes, indicating that some oncofetal lncRNAs in this profile may also play a important role in the development of fetal liver and liver cancer. The GO analysis results were consistent with these findings and were listed in Fig. 1d and Supplementary Figure S1B, C. Thus, our results indicated that there were a series of lncRNAs that were frequently aberrantly expressed in fetal liver and liver cancer tissues compared to the normal liver tissues that might be related to the carcinogenesis process.

Fetal lncRNA Ptn-dt is significantly upregulated in mouse liver cancer tissues

To investigate the relationship among embryonic development, liver cancer and the aberrantly expressed lncRNAs, we further analyzed the microarray results via a bioinformatics analysis. We selected the top 30 differentially expressed genes, which were obtained from the intersection between our 1070 oncofetal lncRNAs as described above and another set of lncRNA microarray data from our previously published work [17], which contains highly expressed lncRNAs in fetal livers (Fig. 1e). Since the purpose of this study was to screen for lncRNAs that are highly expressed in the embryo and fetal stage and simultaneously play a role in liver carcinogenesis, we are more likely to screen lncRNAs that are also upregulated in the fetal livers. Therefore, the 30 differentially expressed genes mentioned above were sorted precisely from high to low in reference to the group of fetal livers, and the results were drawn into a cluster map (Fig. 1f). Among these genes, we noticed one lncRNA, Pleiotrophin downstream transcript (termed lncRNA Ptn-dt, NCBI Accession no. AK161964; UCSC ID uc009biz.1), which was the most significantly highly expressed. To verify the upregulation of Ptn-dt during the embryonic stage and tumorigenesis stage, we detected the expression of Ptn-dt by qRT-PCR in mouse brain, heart, lung, kidney and liver tissue samples in the embryonic stage and adult stage (Fig. 1g). Three samples were used in each group. The result showed that Ptn-dt was highly expressed in multiple organs including liver in embryonic stage compared to that in adult stage. Meanwhile, the expression level of Ptn-dt were further confirmed by qRT-PCR using additional five samples from each group of fetal liver tissues, liver cancer tissues, and normal adult mouse liver tissues respectively (Fig. 1h). We found that the expression of Ptn-dt was remarkably higher in the embryonic tissues and tumor tissues than that in the adult tissues. Then, to confirm the existence of the Ptn-dt transcripts, we detected Ptn-dt in the mouse embryo liver samples, liver cancer tissues, and adult liver tissues by a northern blot analysis (Fig. 1i). The results indicated that Ptn-dt transcripts exists in the genome of the mouse, and the relative content and length of Ptn-dt were similar to the result of qRT-PCR and the UCSC Genome Browser results. Moreover, the RNA fluorescence in situ hybridization (FISH) analysis not only confirmed the differential expression in different liver tissues in mice but also suggested that Ptn-dt was mainly distributed in the cytoplasm (Fig. 1j). Altogether, these findings strongly suggested that fetal lncRNA Ptn-dt was upregulated in mouse liver cancer tissues.

LncRNA Ptn-dt promotes the proliferation of mouse liver cancer cells in vitro

To determine the biological function of lncRNA Ptn-dt in the development of HCC, we conducted gain-of-function and loss-of-function studies in mouse liver cancer cells. We first performed a rapid amplification of cDNA ends (RACE) analysis to identify the 5′ and 3′ ends of the Ptn-dt full-length transcript. Our results indicate that Ptn-dt is an lncRNA located on mouse chromosome 6 downstream of pleiotrophin (Ptn), with a length of 610 bp. The transcription origin and termination sites and sequences of the full-length cDNA of Ptn-dt are presented in Supplementary Figure S2 and Supplementary file 7 in text form. Then, mouse HCC cell lines Hepa1-6 cell lines and Hepa-1c1c7 cell lines with either stably overexpressed Ptn-dt (Fig. 2a) or stably silenced Ptn-dt expression were established (Fig. 2b). Then, we conducted a series of cell proliferation assays in each cell lines using two of the stably transfected clones with invalid control. Ptn-dt was found to enhance cell growth in the CCK-8 assays, indicating that cell proliferation was promoted by Ptn-dt overexpression (Fig. 2c), whereas the knockdown of endogenous Ptn-dt expression inhibited cell proliferation (Fig. 2d).

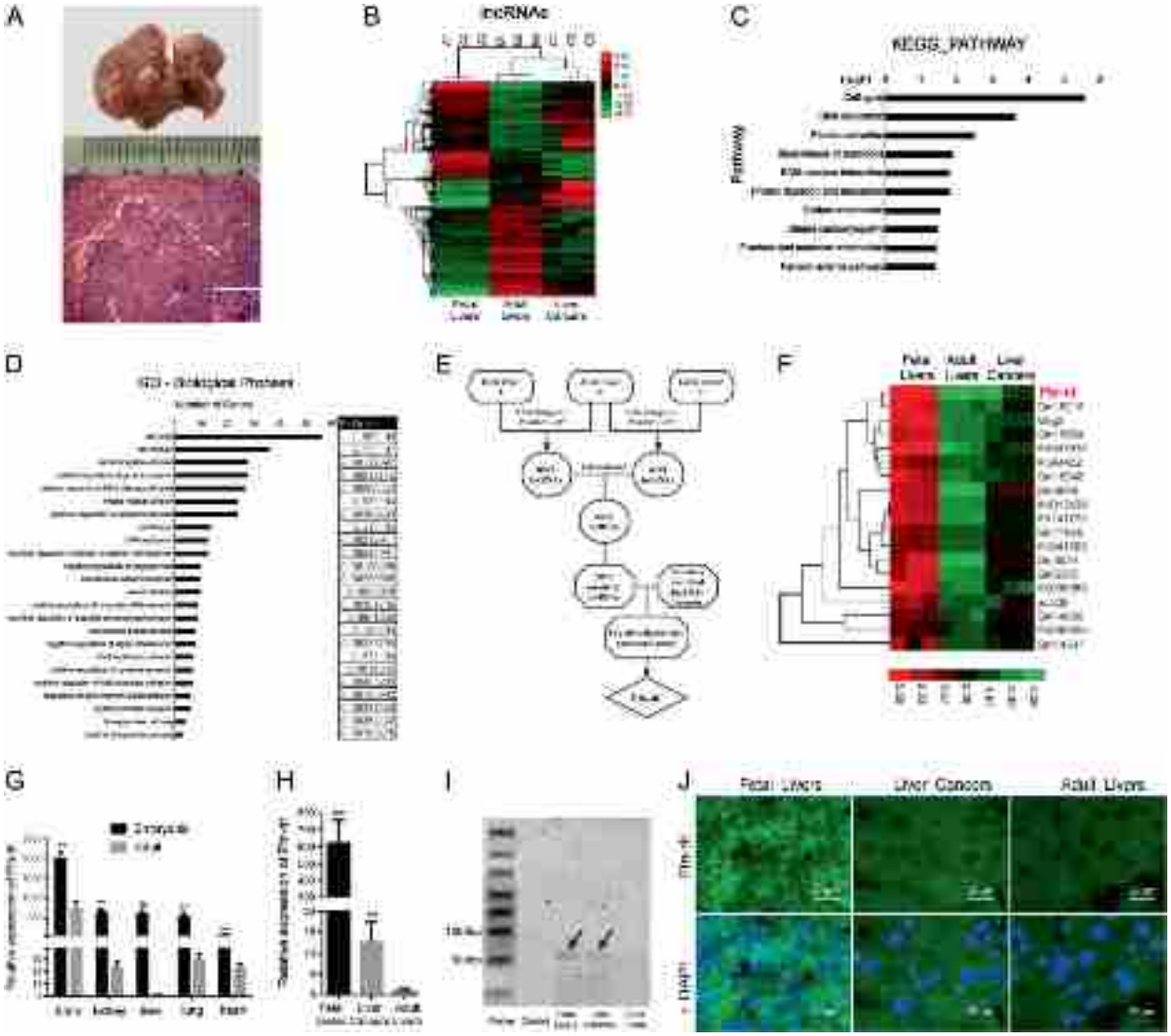

Fig. 1 LncRNA Ptn-dt is overexpressed in mouse liver cancer tissues. **a** In the liver of mice subjected to long-term DEN administration, a macroscopic examination shows multifocal liver cancer nodules (arrows) (upper panel). Photomicrographs of a liver cancer nodule (the lower right) surrounded by normal liver tissue (the upper left) are shown at low (×10) and high (×20) magnifications (lower panel). **b** Hierarchical clustering analysis of lncRNAs that were differentially expressed ($P < 0.05$ and false discovery rate (FDR) < 0.05) in mouse liver samples from fetal livers, adult livers, and liver cancer tissues. Three samples were analyzed at each stage of liver development. The expression values of up and down are represented in shades of red and green, respectively. **c** KEGG pathway analysis showed the significant pathways of 876 differentially expressed oncofetal coding genes, which were highly expressed in both fetal livers and liver cancer tissues from mice compared with the corresponding adult mouse livers ($P < 0.05$). **d** Gene Ontology (GO)-based biological process annotation analysis was used to perform functional enrichment analysis using the DAVID tools. Fold enrichment of the differentially expressed coding genes from 876 differentially expressed oncofetal coding genes, which were highly expressed both in fetal livers and in liver cancer tissues of mice, compared with the corresponding adult mouse livers, is measured by the bar length. The number of genes refers to the number of differentially expressed genes described by biological process annotation. The *P* value represents the significance of the enrichment. Only annotations with a significant *P* value of <0.01 are shown. **e** The flow chart for selecting candidate oncofetal lncRNAs in HCC. **f** A further hierarchical clustering analysis of tissue microarray analysis results showed the representative lncRNAs that were highly expressed in both fetal livers and liver cancer tissues compared with adult mouse liver tissues. **g** qRT-PCR analysis of Ptn-dt expression in different organs of embryonic stage tissue samples and adult stage tissue samples. **h** qRT-PCR analysis of Ptn-dt expression in the livers of mouse fetal stage tissue samples, liver cancer tissue samples, and adult stage tissue samples. **i** Northern blot analysis showed molecular weight and expression levels of Ptn-dt in different tissues. **j** FISH analysis showed colocalization and expression levels of Ptn-dt (green signal, arrows), while the cell nuclei were stained with DAPI (blue signal). Data are shown as the mean ± standard deviation ($n = 3$) and are representative of three independent experiments. $^{**}P < 0.01$ (Student's t test)

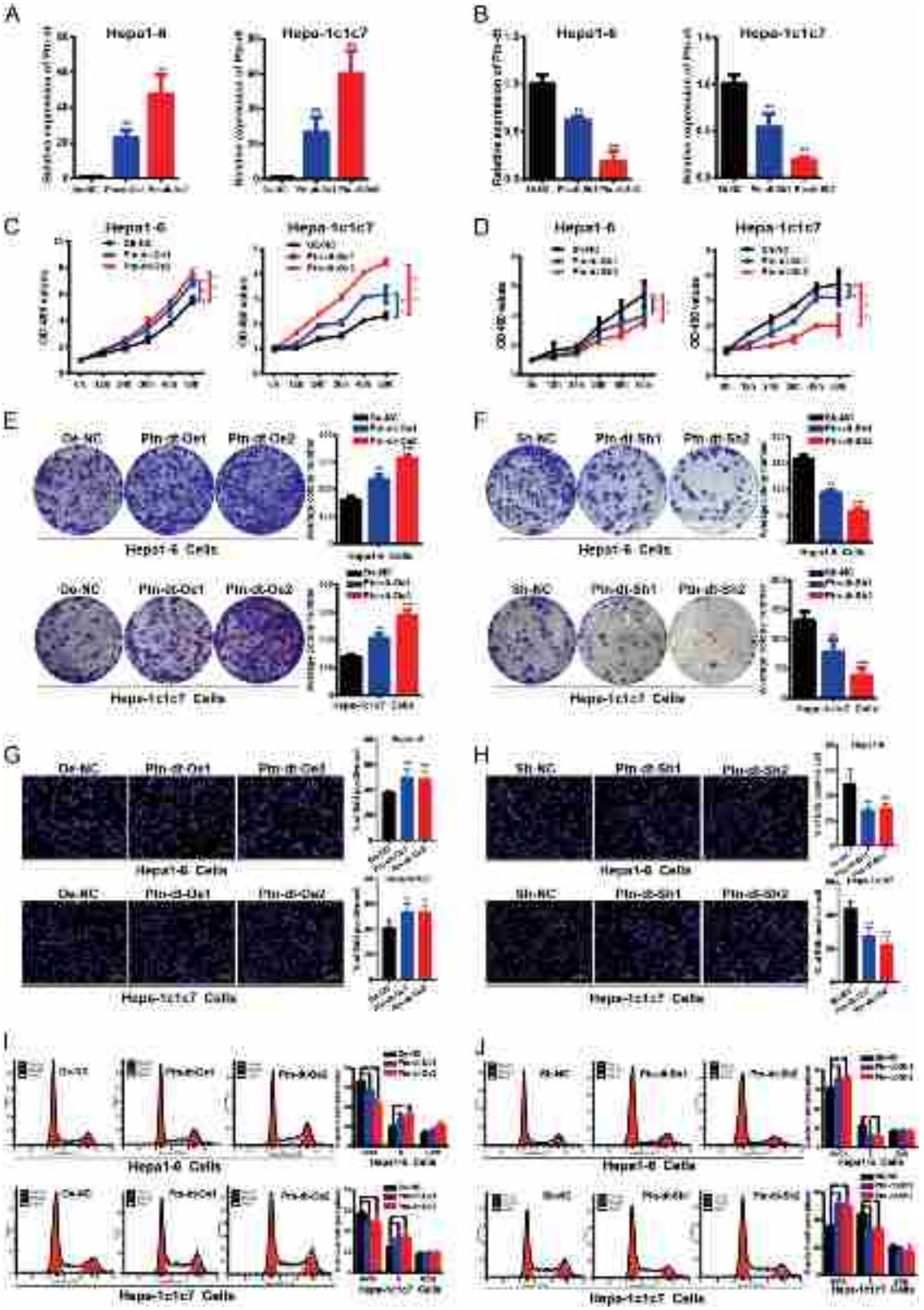

In the colony formation assays, the Ptn-dt-upregulated cell lines displayed more colony formations (Fig. 2e); however, the colony number was much lower in the Ptn-dt downregulated cell lines (Fig. 2f) compared to the control group containing the invalid vector. EdU (5-ethynyl-2′-deoxyuridine) immunofluorescence staining of the Ptn-dt-

◀ **Fig. 2** LncRNA Ptn-dt promotes cell proliferation in vitro. **a** Hepa1-6 and Hepa-1c1c7 cells were infected with lentiviruses carrying the Ptn-dt cDNA, and Ptn-dt stably overexpressing Hepa1-6 and Hepa-1c1c7 cells were screened by qRT-PCR. **b** Ptn-dt expression was detected in the Hepa1-6 and Hepa-1c1c7 cells by qRT-PCR after transduction of lentiviruses encoding Ptn-dt short hairpin RNA (shRNA)−1 or shRNA-2 or a scrambled shRNA. **c** Cell growth rates were determined by performing CCK-8 assays. Ptn-dt overexpression enhanced Hepa1-6 and Hepa-1c1c7 cell proliferation relative to the control cells. **d** Ptn-dt depletion inhibited the proliferation of Hepa1-6 and Hepa-1c1c7 cells. **e**, **f**) Clone formation in Ptn-dt stably overexpressing (**e**) or interfering (**f**) Hepa1-6 and Hepa-1c1c7 and negative control cells. Representative graphs are shown. The graphs depict the count number from three independent experiments. **g**, **h** Ptn-dt overexpressing (**g**) or knockdown (**h**) Hepa1-6 and Hepa-1c1c7 cells were seeded onto coverslips, and cell proliferation was assessed using EdU immunofluorescence staining. The graphs on the right show the percentage of EdU-positive nuclei. The data shown are the means of three independent experiments. Scale bar = 100 μm. **i**, **j** An analysis of the cell-cycle phase distribution by flow cytometry shows significant increases or decreases in cells in the S or G1 phase, respectively, in Ptn-dt overexpressing Hepa1-6 and Hepa-1c1c7 cells (**i**). In contrast, cells in the S-phase population decreased significantly when Ptn-dt was silenced in the Hepa1-6 and Hepa-1c1c7 cells (**j**). $^{*}P < 0.05$, $^{**}P < 0.01$, $^{***}P<0.001$ (Student's *t* test)

overexpressed and Ptn-dt-downregulated stable cell lines revealed higher ratios of EdU-positive nuclei in the former but lower numbers in the latter compared with those in the control cell lines (Fig. 2g, h). Altogether, colony formation assay and EdU cell proliferation assay indicated Ptn-dt could promote cell proliferation in mouse liver cancer cells in vitro.

To explore the mechanism behind this, we analyzed the cell-cycle distributions using fluorescence-activated cell sorting (FACS). The results showed a reduction in the G0/G1 population and an increase in the S-phase population in the Ptn-dt overexpressed Hepa1-6 and Hepa-1c1c7 cells (Fig. 2i); in contrast, the Ptn-dt knockdown cell lines had the opposite effects (Fig. 2j). Therefore, Ptn-dt could accelerate the cell-cycle process and facilitate the cell proliferation in mouse liver cancer cells. Additionally, Ptn-dt-Oe2 and Ptn-dt-Sh2 demonstrated more significant cell proliferation and inhibited cell proliferation compared to Oe-NC and Sh-NC respectively, thus were used in the continuing experiments.

Meanwhile, overexpressing Ptn-dt in normal adult liver cell AML12 could also promote cell proliferation in EdU assays (Supplementary Figure S3A). Furthermore, we used the FACS assay to detect apoptosis in the Ptn-dt overexpressed and knockdown Hepa1-6 and Hepa-1c1c7 cell lines, which were stained with Annexin V-APC/PI. However, no obvious positive result was obtained, i.e., Ptn-dt overexpression had no effect on cellular apoptosis (Supplementary Figure S4A), and the Ptn-dt knockdown also did not affect cellular apoptosis (Supplementary Figure S4B). Collectively, all these data indicated that Ptn-dt could promote cell proliferation in vitro by accelerating cell-cycle progression.

LncRNA Ptn-dt promotes the growth of mouse liver cancer cells in vivo

To obtain insights into the influence of Ptn-dt in hepatocarcinogenesis in vivo, Ptn-dt overexpressed and controlled Hepa1-6 cells labeled with firefly luciferase were injected subcutaneously into the armpits of nude mice. The xenograft tumors grown from cells stably overexpressing Ptn-dt (Fig. 3a, red arrow) had larger mean volumes compared with those produced from controlled xenografts (Fig. 3a, white arrow). The images of nude mice corresponding to Fig. 3a in the xenotransplantation assay using Ptn-dt overexpressed and control cells were shown in Supplementary Figure S4C. The results of the measurements of the tumor volume indicated that the upregulation of Ptn-dt could markedly promote tumor growth (Fig. 3b, c). Ki67, which is a nuclear antigen associated with cell proliferation, was detected using immunohistochemical staining, and the expression of this antigen was prominently upregulated in the Ptn-dt overexpressing group compared with that in the control group (Fig. 3d).

In contrast, we constructed stable Ptn-dt knockdown cells using lentivirus-mediated short hairpin RNA (shRNA). Hepa1-6-luciferase cells infected with Ptn-dt-Sh and control Sh-NC lentiviruses were injected subcutaneously into nude mice. We observed the xenograft growth for 12 days and found that the Ptn-dt depletion could inhibit the tumor growth (Fig. 3e, red arrow) compared with those produced from control xenografts (Fig. 3e, white arrow). The results of the measurements of tumor volume indicated that the Ptn-dt depletion could markedly inhibit the tumor growth (Fig. 3f, g). Compared with those produced from the control xenografts, there was a low level of Ki67 in the Ptn-dt-depleted xenograft tumor tissues (Fig. 3h). Altogether, the above-mentioned results demonstrated that Ptn-dt could enhance mouse liver cancer cell proliferation in vivo.

LncRNA Ptn-dt interacts with RNA-binding protein HuR

It is well known that the functions of lncRNAs are closely related to their subcellular distribution. We have recognized that lncRNA Ptn-dt mainly located in the cytoplasm (Fig. 1j). In addition, several studies have shown that cytoplasmic lncRNAs regulate gene transcription mainly by interacting with RNA-binding proteins [18]. Thus, we used RNA pulldown assays to search for proteins in the cytoplasm interacting with Ptn-dt. In the RNA pulldown assays, Ptn-dt or truncated Ptn-dt and its antisense RNA were used to incubate with Hepa1-6 cells extracts. Bands that were

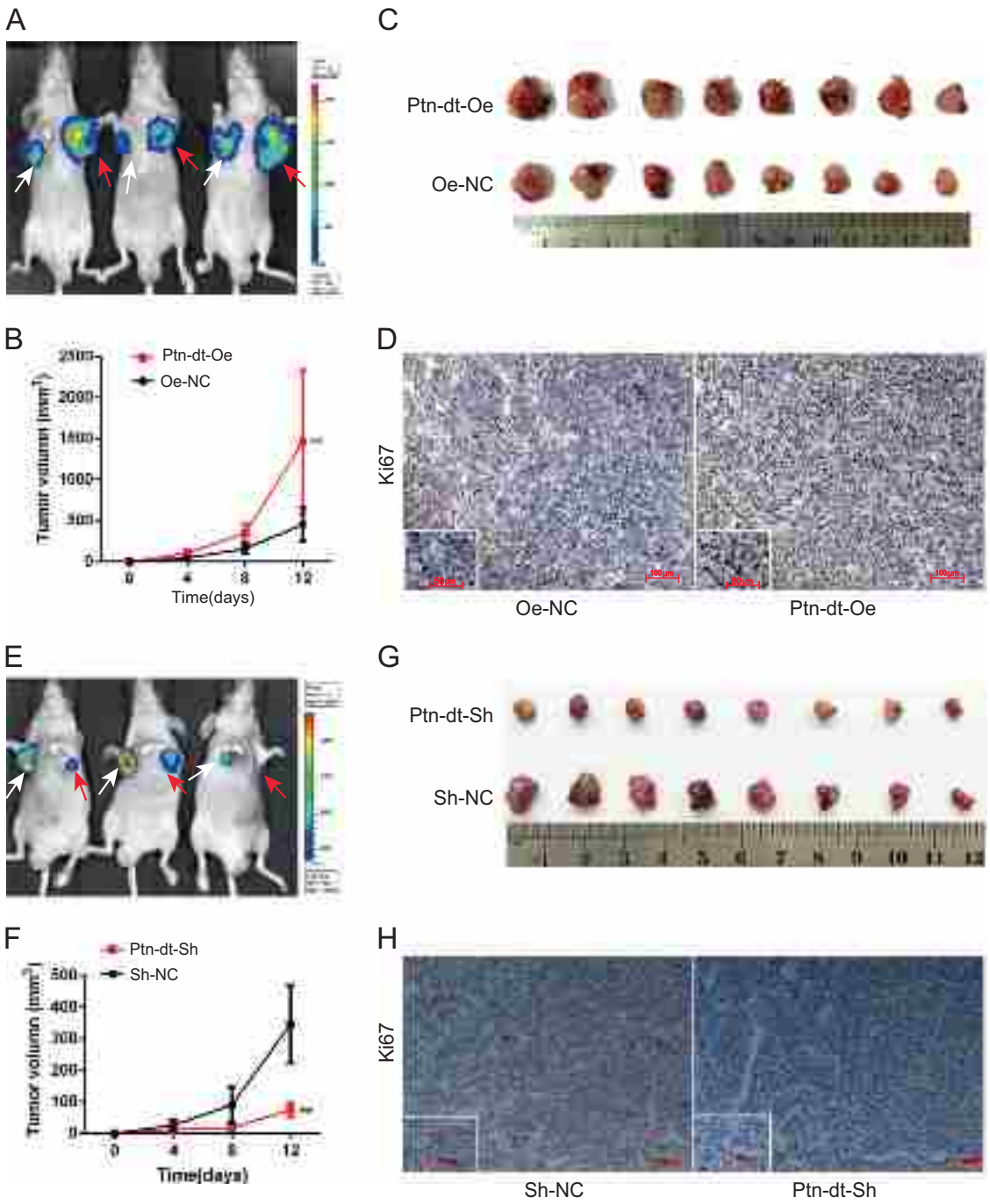

specific to Ptn-dt were removed and subjected to mass spectrometry (Fig. 4a). HuR (Elavl1, ELAV-like protein 1) and G3P (Gapdh, Glyceraldehyde-3-phosphate dehydrogenase) were the main proteins recognized by the mass spectrometry that interacted with Ptn-dt (Supplementary Table S1). Because HuR is an RNA-binding protein that can stabilize many RNA molecules and regulate their transcription [19], we initially selected HuR to further validate its interaction with Ptn-dt. Then, we used western blot assays to examine the level of HuR protein obtained by the above-mentioned RNA pulldown assays. The results showed that compared with the antisense group, HuR was enriched in the sense strand group (Fig. 4b). Furthermore, anti-HuR RIP followed by PCR also confirmed the enrichment of Ptn-dt by the anti-HuR antibody compared with IgG (Fig. 4c). Moreover, HuR was shown to bind the 5′-end (1–350 nt) of Ptn-dt through truncated Ptn-dt pull-down assays (Fig. 4d). Altogether, these findings indicated that Ptn-dt could interact with the protein HuR at the 5′-end.

◀ **Fig. 3** Lnc RNA Ptn-dt accelerates the growth of Hepa1-6 cells in vivo. **a**–**d** Subcutaneous tumor model of Ptn-dt overexpressing Hepa1-6-luci cells ($n = 8$ for both groups). **a** Photographs of tumors that developed in xenograft-transplanted nude mouse tumor models viewed using the IVIS Imaging System (Caliper Life Sciences, Hopkinton, MA). The luciferase signals were captured in the nude mouse models 12 days after the injection of Ptn-dt overexpressing (red arrow) or control (white arrow) Hepa1-6 cells. **b** Tumor growth curves in mice over time after the subcutaneous injection of 1×10^6 of Ptn-dt overexpressing or control Hepa1-6-luci cells. **c** Images of xenografts established by SC transplantation with Ptn-dt overexpressing and control Hepa1-6-luci cells 12 days after the cell injection ($n = 8$, $P < 0.01$). **d** IHC staining shows that the expression of Ki67 was enhanced in the Ptn-dt overexpressing group compared to the control group. The higher magnification is shown on the left bottom of each part. Original magnification ×200. **e**–**h** Subcutaneous tumor model of stable Ptn-dt-interference Hepa1-6-luci cells ($n = 8$ for both groups). **e** Representative photographs of mice by imaging using the IVIS Imaging System. The luciferase signals were captured in the nude mouse models 12 days after the injection of Ptn-dt-silencing (red arrow) or control (white arrow) Hepa1-6-luci cells. **f** Tumor growth curves. Tumors induced by Ptn-dt silencing in Hepa1-6-luci cells showed markedly lower growth rates than the control cells. **g** Representative images of tumors formed in nude mice injected subcutaneously with the Ptn-dt-silencing Hepa1-6-luci cells. **h** IHC staining shows that the expression of Ki67 was enhanced in the Ptn-dt-silencing group compared to the control group. The lower magnification is shown on the left bottom of each part. Original magnification ×200. $^{**}P < 0.01$ (Student's *t* test)

To explore the effects of lncRNA Ptn-dt on HuR, we tested the expression of HuR at both the mRNA and protein level in the Ptn-dt control and overexpressing Hepa1-6 cells. The results showed that the overexpression of Ptn-dt had no effect on the expression of HuR at either the mRNA (Fig. 4e) or protein level (Fig. 4f). Therefore, these results confirmed that there was an interaction between Ptn-dt and HuR, but Ptn-dt did not affect the expression of HuR.

LncRNA Ptn-dt promotes the proliferation of mouse liver cancer cells through the HuR/miR-96/Alk pathway and Ptn-Alk axis

To clarify the interaction between Ptn-dt and HuR, we noticed that some previous studies have reported that HuR, as an RNA-binding protein, could stabilize many mRNAs and regulated their translation through interacting with microRNAs, such as miR-34a [20], miR-125a [21], miR-122 [22], miR-16 [23], miR-96 [24], etc. [19]. Thus, we tested the expression of those microRNAs by RIP assays using anti-HuR in Hepa1-6 cell extracts (Fig. 5a), and the results indicated that miR-96 could bind with HuR and possessed the largest enrichment among these group of microRNAs in RIP.

Protein Ptn is a heparin-binding growth factor with diverse biological activities, including promoting proliferation of tumor cells [25]. On chromosome, lncRNA *Ptn-dt* is located downstream of *Ptn* with a gap of 129 bases (Fig. 5b), and the northern blot analysis (Fig. 1g) indicated that Ptn-dt and Ptn were two independent transcripts. To examine the relationship between lncRNA Ptn-dt and Ptn, we detected the expression levels of Ptn in the stably transfected Ptn-dt overexpressing cell line by qRT-PCR and showed that there were no direct effects on Ptn expression when Ptn-dt was overexpressed (Fig. 5c). Then, we targeted Anaplastic lymphoma kinase (Alk), which is a transmembrane receptor of Ptn [26, 27]. We then tested the expression of Alk at the mRNA and protein level in Ptn-dt overexpressing Hepa1-6 cells. The results showed that overexpression of Ptn-dt could enhance Alk expression at the mRNA level (Fig. 5d) and protein level (Fig. 5e). The Alk protein was detected in the form of EML4-ALK v1 (MW:117 kDa). In vivo, the xenograft tumor samples of Oe-NC and Ptn-dt-Oe were examined for Ptn-dt and Alk expression using real-time PCR. Elevated Ptn-dt level in xenograft tumor samples could upregulate Alk expression in vivo (Fig. 5f, g).

As previously reported by Vishwamitra et al. [24], miR-96 is a posttranscriptional suppressor of Alk. To investigate whether Ptn-dt influenced the expression of miR-96, we tested the expression of miR-96 by qRT-PCR assays, and the results showed that the expression of miR-96 was lower in the cells with Ptn-dt overexpression than that in the control cells (Fig. 5h). Meanwhile, when knocking down Ptn-dt, Alk protein levels were significantly decreased and miR-96 was upregulated (Fig. 5i, j). Furthermore, to confirm the posttranscriptional inhibition of miR-96 on Alk, we used double-stranded microRNA oligonucleotide mimics in the Hepa1-6 cells to overexpress miR-96 (Fig. 5k) and then assessed the expression of Alk using qRT-PCR and western blot assays. The results indicated that Alk was downregulated at the protein level (Fig. 5l) but not at the mRNA level. Meanwhile, we inhibited miR-96 with antisense oligonucleotide inhibitors (Fig. 5m) and then assessed the expression of Alk by qRT-PCR and western blot assays. Consistent results were obtained after the miR-96 inhibition in which Alk was upregulated at the protein level (Fig. 5n), and there was no effect at the mRNA level. These results confirmed that miR-96 was a posttranscriptional suppressor of Alk.

To further validate the impact of miR-96, we transfected double-stranded microRNA oligonucleotide mimics miR-96 and mimics-NC to Hepa1-6 Ptn-dt-Oe2 cells. EdU cell proliferation assays results showed that mimics-96 could reverse the effects of overexpressing Ptn-dt on cell proliferation compared to the control group (Fig. 5o). Also, the antisense oligonucleotide inhibitors of miR-96 and inhibitors NC were transfected to Hepa1-6 Ptn-dt-Sh2 cells. The results should that inhibiting miR-96 could compensate the proliferation postponement of knocking down Ptn-dt (Fig. 5p).

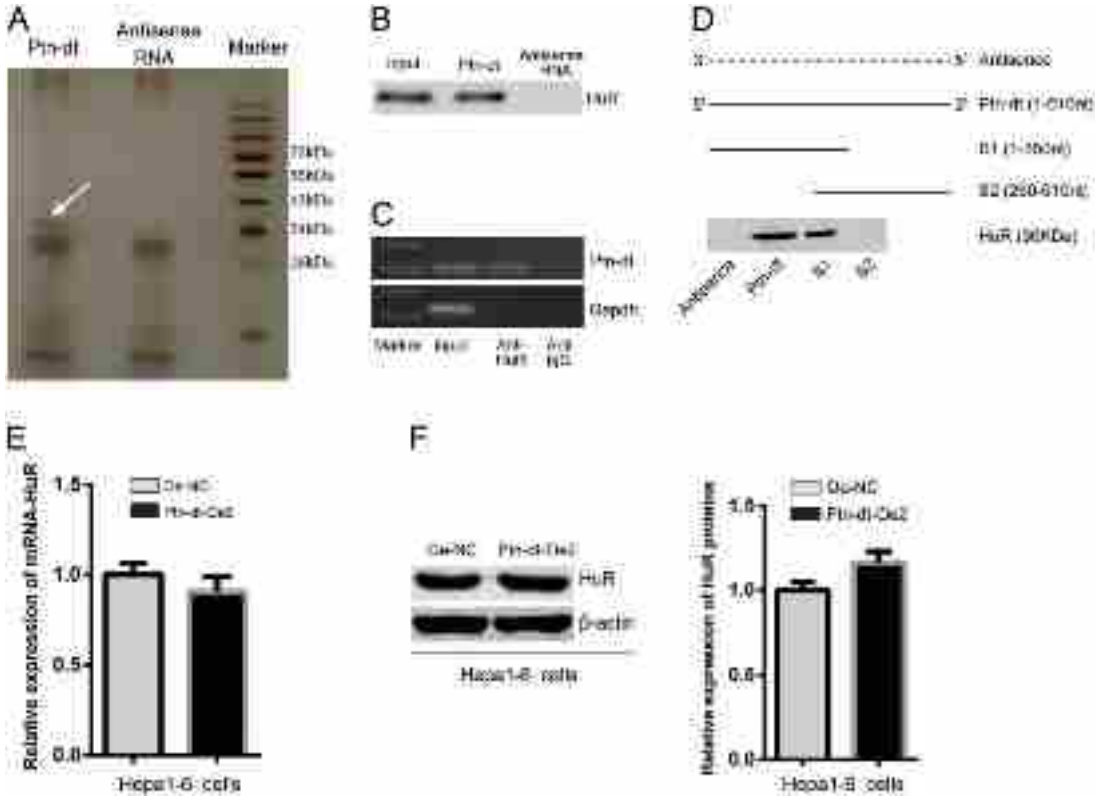

Fig. 4 LncRNA Ptn-dt can interact with RNA-binding protein HuR and increase its protein expression level. **a** Silver-stained SDS-PAGE gel of proteins immunoprecipitated from Hepa1-6 cell extract by Ptn-dt and its antisense RNA. The arrow indicates the region of the gel excised for the mass spectrum determination by the liquid chromatography dual mass spectrometry method. **b** The protein HuR was found by mass spectrometry analysis and was detected by a western blot assay using an anti-HuR antibody. HuR proteins were confirmed in the samples pulled down by Ptn-dt. **c** Relative RIP experiments were performed using an antibody against HuR on extracts from Hepa1-6 cells with IgG as a negative control. The purified RNA was used for the qRT-PCR analysis, and the enrichment of the Ptn-dt was normalized to the input. **d** RNA pull-down of truncated Ptn-dt to confirm HuR-binding sites, and western blot analysis showed the specific association of HuR and Ptn-dt. **e** The mRNA levels of HuR were detected in Ptn-dt upregulated Hepa1-6 cells by qRT-PCR analysis. **f** The protein levels of HuR were detected in Ptn-dt upregulated Hepa1-6 cells by the western blot analysis (left panel). The intensities of the bands from the western blot analysis were quantified by densitometry (right panel).

As previously reported by Kaur et al. [28], the fungal natural product azaphilone-9 bound to HuR and inhibited the HuR-RNA interaction in vitro. Therefore, based on the above findings, we initially speculated that the interaction between Ptn-dt and HuR might affect the binding of HuR and miR-96, and then decreases the stability of miR-96 and reduce the effectiveness of miR-96, which weakened the posttranscriptional inhibition of miR-96 on Alk. In addition, Ptn could activate Alk [29], and Ptn promoted tumor growth and vascular abnormalization via Alk signaling [30]. Our results confirmed that Ptn-dt can positively affect Alk protein expression and promote HCC cell proliferation. Therefore, we further concluded that Ptn-dt could promote tumor cell proliferation via upregulation of Alk and consequently enhance the biological function of Ptn. All in all, Ptn-dt might promote the proliferation of mouse liver cancer cells through the HuR/miR-96/Alk pathway and Ptn-Alk axis (Fig. 6).

Human ortholog RNA of Ptn-dt is identical to long noncoding RNA

Sequence homolog analysis indicated that Ptn-dt was a highly evolutionarily conserved lncRNA in mammals (Fig. 7a), and the alignment revealed that the murine Ptn-dt most likely has a human ortholog RNA, which was referred to as hPTN-DT and was located on human chromosome 7 (chr7:137,227,348–137,228,077) (Fig. 7b). We identified the 5′ and 3′ transcription start and termination sites of the hPTN-DT transcript by RACE analysis; the sequences of full-length hPTN-DT are presented in Supplementary file 7. Analysis of the sequences using ORF Finder proved that hPTN-DT failed to translate into a protein of more than 24 amino acids, the longest ORF of hPTN-DT was 75 bp (Fig. 7c). Prediction of the protein-coding potency of hPTN-DT was carried out using Coding Potential Assessment Tool (CPAT) and Coding Potential Calculator (CPC). Coding probability of hPTN-DT was very low in CPAT,

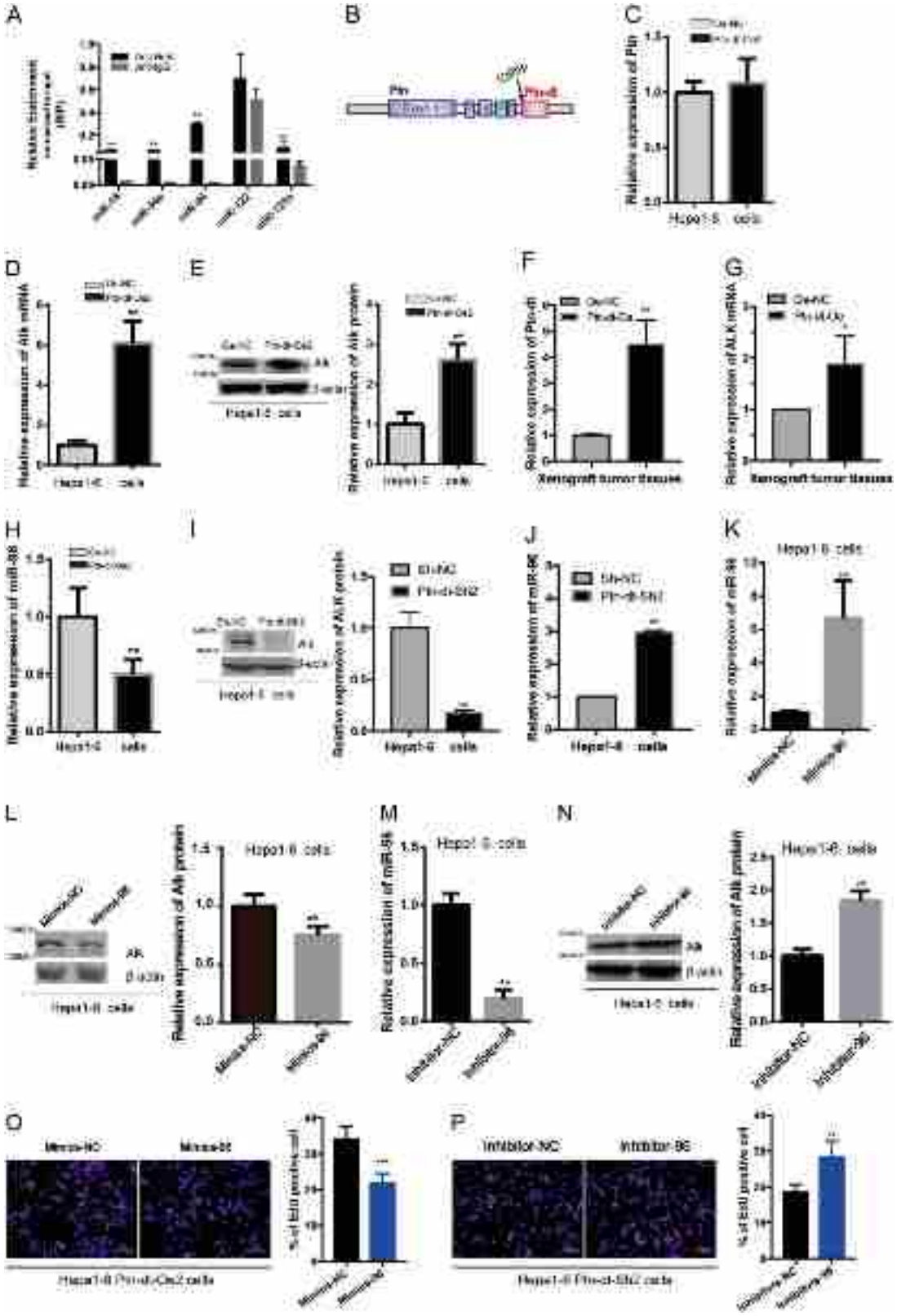

and the coding potential score was negative in CPC. Therefore, we considered hPTN-DT is very likely to be an lncRNA. Moreover, it did not contain a valid Kozak sequence, suggesting the unlikelihood of translation. Thus, the hPTN-DT transcript is identical to lncRNA, and as a

◀ **Fig. 5** The biological function of LncRNA Ptn-dt was dependent on the Ptn receptor Alk. **a** Relative RIP experiments were performed using an antibody against HuR on extracts from Hepa1-6 cells with IgG as a negative control. MicroRNA qRT-PCR for assessing microRNAs endogenously associated with HuR, and the enrichment of miRNAs was normalized to the input. MiRNA-96 held the largest enrichment among the microRNAs. MiRNA-122 had strong non-specific binding to HuR. **b** Diagram showing the position relationship between Ptn-dt and Ptn in the mouse genome. **c** The mRNA expression levels of Ptn were detected in the Ptn-dt upregulated Hepa1-6 cells by qRT-PCR analysis. **d** The mRNA expression levels of Alk were detected in the Ptn-dt upregulated Hepa1-6 cells by qRT-PCR analysis. **e** The protein expression levels of Alk were detected in the Ptn-dt upregulated Hepa1-6 cells by the western blot analysis (left panel). The intensities of the bands from the western blot analysis were quantified by densitometry (right panel). **f**, **g** The expression level of Ptn-dt and Alk in xenograft tumor tissues of Oe-NC and Ptn-dt-Oe was identified by qRT-PCR. Ptn-dt-Oe tumor tissues showed elevated Ptn-dt levels and Alk levels. **h** The expression levels of miR-96 were detected in Hepa1-6 cells with Ptn-dt over-regulation by qRT-PCR analysis. In Ptn-dt-Oe2 cells, miR-96 was downregulated. **i** The protein expression levels of Alk were detected in the Ptn-dt downregulated Hepa1-6 cells by the western blot analysis (left panel). The intensities of the bands from the western blot analysis were quantified by densitometry (right panel). Alk was significantly downregulated in Hepa1-6 Ptn-dt-Sh2. **j** The expression levels of miR-96 were detected in Hepa1-6 cells with Ptn-dt downregulation by qRT-PCR analysis. In Ptn-dt-Sh2 cells, miR-96 was upregulated. **k** Overexpression efficiency of miR-96 in Hepa1-6 cells, which were screened by qRT-PCR analysis. **l** The protein expression levels of Alk were detected in the Hepa1-6 cells with miR-96 overexpression by the western blot assays. **m** Knockdown efficiency of miR-96 in Hepa1-6 cells, which were screened by qRT-PCR analysis. **n** The protein expression levels of Alk were detected in the Hepa1-6 cells with the knockdown of miR-96 by western blot assays. **o** Double-stranded microRNA oligonucleotide mimics of miR-96 and mimics-NC were transfected to Hepa1-6 Ptn-dt-Oe2 cells, and cell proliferation was examined by EdU assays. **p** Antisense oligonucleotide inhibitors of miR-96 and inhibitors NC were transfected to Hepa1-6 Ptn-dt-Sh2 cells, and cell proliferation was examined by EdU assays. $*P < 0.05$, $**P < 0.01$ (Student's *t* test)

human ortholog of Ptn-dt, it may also share similar properties in the pathogenesis of human HCC.

Discussion

HCC is the fifth most common cancer in men and the seventh most common cancer in women. Even though medical treatment has constantly been advancing, the mortality rate of HCC patients remains high, ranking as the second most frequent cause of cancer death in men and the seventh most frequent cause of death in women [31]. Therefore, there is an urgent need to explore the molecular mechanism of hepatocarcinogenesis and develop accurate treatments. In cancer biology, a cancer cell is similar to an embryonic cell as follows: both cell types have extraordinary plasticity, and their proliferation, migration, invasiveness and the ability to make metabolic adjustments share common molecular pathways and exhibit similar epigenetic patterns [32]. In particular, oncofetal genes, which have the gene expression characteristics of embryonic stem cells and progenitor cells, are a type of tumor markers with unique importance. LncRNAs are a subgroup of noncoding RNAs with a length of more than 200 nucleotides. It is increasingly evident that lncRNAs play an important role in embryonic development and the genomic mutations in cancer. Recent papers have implied that dysregulation of certain lncRNAs may also affect the genomic regulation over cell signaling pathways and provide a cellular growth advantage, leading to uncontrolled tumor growth [33]. Although many lncRNAs have been identified, there are only a few functionally characterized lncRNAs. Thus, the purpose of this study was to identify more oncofetal lncRNA molecules that may be potentially used in the diagnosis and treatment of HCC patients through the screening of lncRNAs microarray. In this study, we analyzed the expression profiles of lncRNA from fetal livers, adult livers and liver cancer tissues from male mice by microarray. Notably, numerous lncRNAs showed a higher expression in both the fetal liver and liver cancer tissues, which indicates that this gene network is more active during fetal liver development and hepatocarcinogenesis. It is well known that liver regeneration and hepatocarcinogenesis involve some of the same transcription factors, cytokines, and signaling pathways as in fetal liver development [34]. In our previous work, we showed that lncRNA H19, an oncofetal gene, inhibited the proliferation of fetal liver cells through blocking the interaction between heterogeneous nuclear ribonucleoprotein U and actin [35], and lncRNA-LALR1 accelerated hepatocyte proliferation during liver regeneration [36]. Thus, we focused on the fetal liver-specific and liver cancer-specific lncRNAs and explored their molecular characteristics and biological functions.

Ptn, which is an 18-kDa heparin-binding cytokine, is secreted by a 136 amino acid and has pleiotropic effects, including differentiation, angiogenesis, and mitogenesis [37]. The *Ptn* gene, which is a proto-oncogene tumor promoter, participates in the regeneration and development of the liver [38] through its receptor proteins, such as Alk [39], and protein tyrosine phosphatase beta/zeta (RPTP β/ζ) [40]. In this study, we identified the oncofetal lncRNA Ptn-dt, which is located downstream of *Ptn* at a distance of 129 bases. The northern blot analysis (Fig. 1g) showed that Ptn-dt is an independent transcript in the mouse genome. In the results of our microarray (Fig. 1d), Ptn-dt was significantly upregulated in the mouse fetal liver and liver cancer tissues compared with that in the control adult mouse liver tissues. Moreover, a series of in vivo and in vitro experiments confirmed that Ptn-dt could promote cell proliferation during the process of mouse hepatocarcinogenesis. These results indicated that lncRNA Ptn-dt could be a critical regulator of hepatocyte proliferation during mouse fetal liver development and hepatocarcinogenesis.

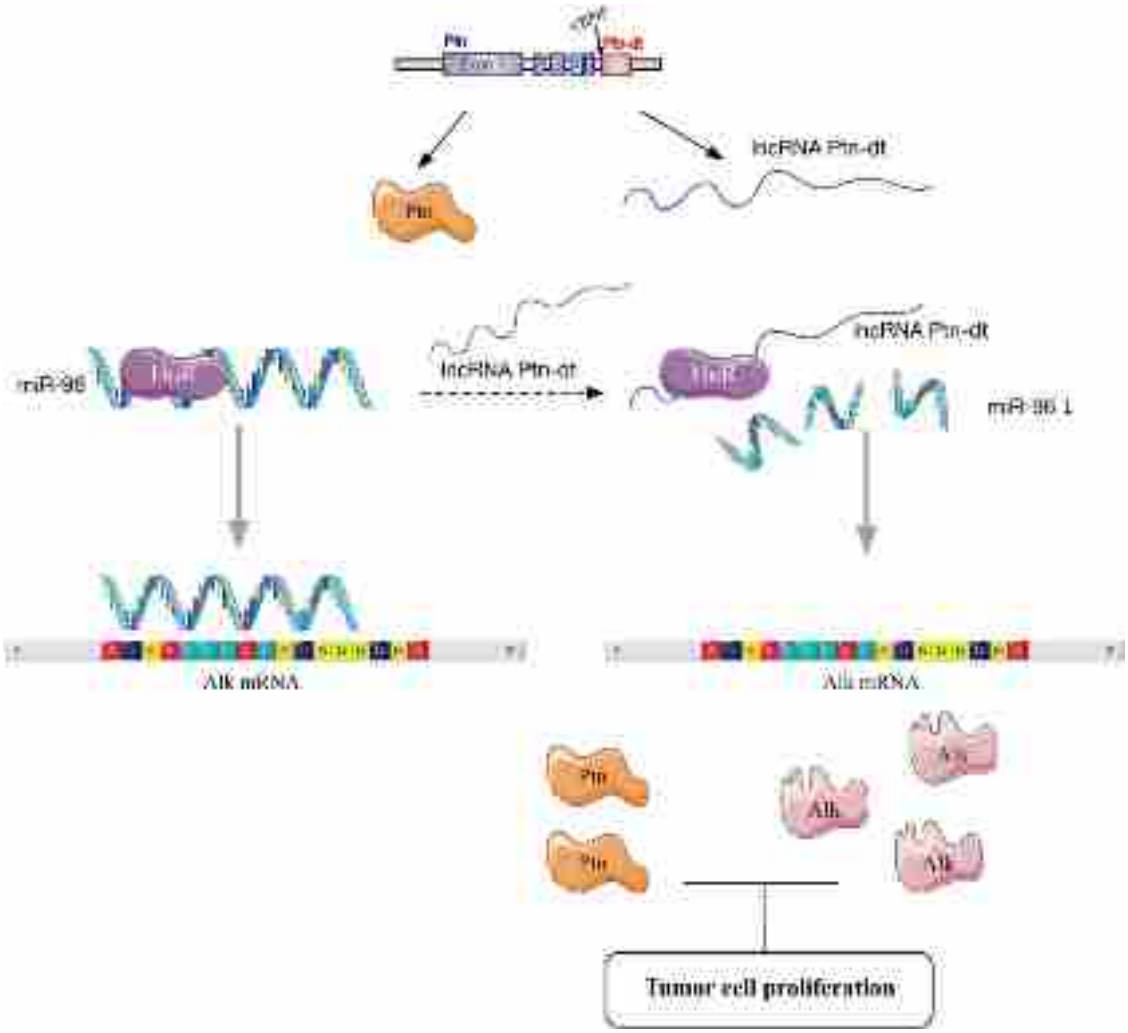

Fig. 6 LncRNA Ptn-dt promotes the proliferation of mouse liver cancer cells through the HuR/miR-96/Alk pathway and Ptn-Alk axis. LncRNA *Ptn-dt* is located at the downstream of the protein-coding gene *Ptn*. LncRNA Ptn-dt regulates the function of Ptn through the HuR/miR-96/Alk pathway as follows: Ptn-dt, by interacting with an RNA-binding protein HuR, affects the binding of HuR with miR-96, leading to the decreased stability of miR-96. The reduced amount of miR-96 consequently leads to weakened posttranscriptional inhibition on Alk, which is a transmembrane receptor of Ptn. Previous studies have identified that Ptn promotes tumor growth and vascular abnormalization via Alk signaling. Therefore, lncRNA Ptn-dt promotes the proliferation of mouse liver cancer cells through the HuR/miR-96/Alk pathway and Ptn-Alk axis

The importance of lncRNAs in mammalian diseases can be attributed to their ability to impact cellular functions through different mechanisms. Increasing evidence has shown that lncRNAs drive carcinogenesis by promoting cell proliferation via the regulation of critical proteins, such as PCAT-1 [41], RN7SK [42], and SRA [43]. Some recent studies have found that a subset of lncRNAs enriched in the cytoplasm regulated mRNA stability [44], mRNA translation [45], and protein localization [46]. The potential mechanisms of some well-defined lncRNAs are profoundly understood, such as HOX transcript antisense RNA (HOTAIR; in postural identity), and X inactive specific transcript (XIST; in X chromosome inactivation) [12]. LncRNAs might act through a wide range of mechanisms, which would be consistent with their properties of subcellular localizations, expression levels, and stabilities identified in lncRNAs in mammalian cells [47]. For instance, the functional mechanisms of lncRNAs can act through genomic targeting, including acting on their neighboring genomic environment (in *cis*) and diffusing to distant sites of action (in *trans*). Innovatively, in this study, we found another mechanism of action of lncRNAs, namely, lncRNA functions by acting on the receptor of its adjacent protein-coding gene. We found that lncRNA Ptn-dt was expressed mainly in the cytoplasm and interacted with HuR, an RNA-binding protein, and could regulate the transcription and translation of many target mRNAs through affecting the interaction between HuR and microRNAs [48]. Meanwhile, the overexpression of Ptn-dt could upregulate Alk protein expression. Alk was also found to be

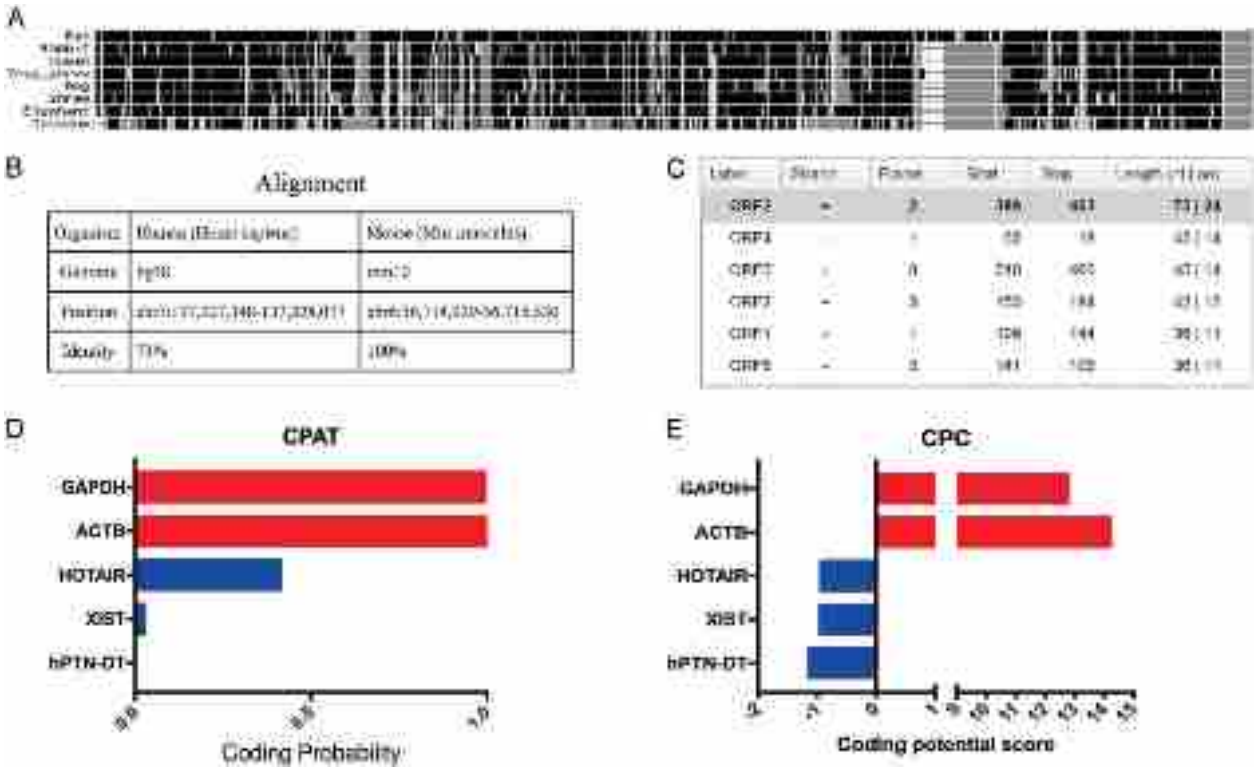

Fig. 7 Human orthlog RNA of Ptn-dt is identical to long noncoding RNA. **a** Alignment of the cDNAs of *Ptn-dt* from each species shows that it is conserved in mammals. **b** Alignment revealed that the murine lncRNA Ptn-dt most likely has an ortholog RNA on human chromosome 7 with the best sequence similarity as 73%. **c** Putative proteins possibly encoded by hPTN-DT as predicted by ORF Finder. The predicted proteins were subjected to Blastp search and are consistent with noncoding. **d** Coding probability of hPTN-DT as predicted by CPAT. **e** Coding potential score of hPTN-DT as predicted by CPC

regulated by miR-96 and is known to be a downstream target of Ptn. Currently, based on our findings, we assume that the upexpression of lncRNA Ptn-dt impacts the binding of HuR with miR-96, therefore decreases the stability of miR-96, and eliminates the post-transcriptional inhibition of miR-96 on Alk; eventually, the upregulation of Alk enhances the biological function of Ptn and promotes cell proliferation. Further research can be conducted to elucidate other possible effects and mechanisms of Ptn-dt on the occurrence and development of HCC.

Additionally, we identified a human ortholog RNA of Ptn-dt, hPTN-DT, which was also an lncRNA. By inference, hPTN-DT may also participate in the pathogenesis of human HCC through a similar mechanism of Ptn-dt. However, these inferences need further experimental verification in human cell lines and tissues.

Altogether, we provided an efficient way to screen for valuable oncofetal molecules associated with HCC. Furthermore, our study was the first to demonstrate that lncRNA Ptn-dt acted as a regulator in HCC progression. Most importantly, we found a new mechanism of action of lncRNA as follows: lncRNAs may exert their functions by regulating the receptor of its adjacent protein-coding gene. Nevertheless, further studies are essential to comprehensively understand the detailed functions and mechanisms of lncRNA Ptn-dt in the occurrence and development of HCC and as an effective target for the prevention, diagnosis, and treatment of HCC patients.

Materials and methods

Acquisition of mouse tissue samples and microarray analysis

C57BL/6 mice were bred in the common animal house at the Department of Medical Genetics, Second Military Medical University. All experimental procedures on mice were approved by the Institutional Animal Care and Use Committee of the Second Military Medical University, Shanghai, China. The female mice were sacrificed at 17.5 days of pregnancy, and embryonic liver tissues were carefully separated from the fetal male mice and quickly frozen in liquid nitrogen. Adult liver tissues were obtained from 8-week-old male C57BL/6 mice. Liver cancer samples were harvested from liver cancer mouse models, which were subjected to intraperitoneal injections of the chemical carcinogen diethylnitrosamine (DEN) at the dose of 25 mg/kg of BW on the 15th day after the birth of

the male C57BL/6 mice, and among which approximately 80% developed liver cancer after 1 year. There was no blinding and randomization. Each group of these samples had three biological replicates. Total RNA from these three groups of mouse liver samples was isolated, amplified and transcribed into fluorescent complementary RNA (cRNA) using the Agilent Quick Amp Labeling Kit (Palo Alto, CA, USA). The labeled cRNAs were then hybridized onto the Mouse LncRNA Array 2.0 (8 × 60 K, ArrayStar, Rockville, MD), and after the washing steps, the arrays were scanned by an Agilent Scanner G2505B. Agilent Feature Extraction software (version 10.7.3.1) was employed to analyze the acquired array images. The quantile normalization and subsequent data processing were conducted using GeneSpring GX v11.5.1 software package (Agilent Technologies). The differentially expressed lncRNAs and mRNAs with statistical significance were identified and illustrated using volcano plot filtering. The threshold set to screen the upregulated or downregulated genes was fold-change > 2.0 and P value < 0.05.

RNA isolation, reverse transcription reactions, and qRT-PCR

Total RNA was extracted by the RNAiso Plus (TakaRa Bio Inc.). The first-strand cDNA was generated making use of the PrimeScriptTM RT Master Mix (TakaRa Bio Inc.). Quantitative real-time PCR (qRT-PCR) was conducted using a standard TaqMan qRT-PCR protocol in a StepOne Plus system (Applied Biosystems, Foster City, CA). Gapdh was used as an endogenous control to normalize the amount of total mRNA in each sample. The qRT-PCR reactions of each sample were performed in triplicate. The relative expression of lncRNAs, miRNAs, and protein-coding RNAs was calculated using the comparative $2^{-\Delta\Delta Ct}$ method. All the TaqMan primers and probes were purchased from GenePharma Company (Shanghai, China) and detailed sequences are listed in Supplementary Table S2.

Northern blot analysis

Total RNA was extracted and purified from mouse fetal liver and liver cancer tissues with an SV Total RNA Isolation System (Promega) according to the manufacturer's instructions. A total of 10 μg of the purified RNA was subjected to formaldehyde gel electrophoresis and transferred to a Biodyne Nylon membrane (Pall). A Biotin RNA labeling Mix (Roche) labeled Ptn-dt complementary DNA (cDNA) probe was prepared using PCR. The PCR primers were as follows: sense, AATTCGAGCTCGGTACCC GGGGATCCTTTTGTTTTTGTTTTTGTTTTTTTTAAT GTATACC; Antisense, CCAAGCTTGCATGCCTGCAG GTCGACTTAATTCAG CATCACTTGTT. After 120 min of prehybridization in ULTRAhyb Ultrasensitive Hybridization Buffer (Ambion), the membrane was hybridized for 16 h at 68 °C in ULTRAhyb Ultrasensitive Hybridization Buffer containing the denatured probe. Washes were performed as described in the NorthernMax Kit protocol (Ambion), and the membrane was detected using an Odyssey infrared scanner (Li-Cor, Lincoln, NE).

RNA fluorescence in situ hybridization (RNA FISH)

We performed FISH assays to detect the presence of Ptn-dt using a probe (5′-CTTTGAAAGTTTGCAGACTGA-GAGGAGAGAGGCAGAGCAACG-3′) labeled with FAM fluorescent groups in its 3′ end. The nucleus of 4′,6-diamidino-2-phenylindole (DAPI) was the blue light, and the positive expression was the green light with the corresponding fluorescein labeled.

5′ and 3′ rapid amplification of cDNA ends (RACE)

The 5′-RACE and 3′-RACE were performed to determine the transcriptional initiation and termination sites of Ptn-dt using a GeneRacerTM Kit (RLM-RACE, Invitrogen) according to the manufacturer's instructions. The Ptn-dt primers used for the PCR of the RACE analysis were as follows: 5′-ATGCATTTCTCTCCAATAGAATGAT-3′ (5′RACE) and 5′-GAGAGGCAGAGCAACGATGTAGTG-3′ (3′RACE).

Cell cultures

Mouse hepatoma cell line Hepa1-6, Hepa-1c1c7 and mouse normal liver cell line AML12 were kindly provided by Stem Cell Bank, Chinese Academy of Sciences.

Hepa1-6, Hepa-1c1c7, and Hepa1-6-luci were cultured in Dulbecco's modified Eagle's medium (DMEM) (Hyclone, Thermo) supplemented with 10% fetal bovine serum (FBS) and were maintained in a humidified atmosphere of 5% CO_2 at 37 °C. AML12 complete growth medium was provided from Stem Cell Bank, Chinese Academy of Sciences. The detail formula is as follows (100 ml): DMEM/F-12 (1:1) (Invitrogen, 11330-032) 89 ml, ITS Liquid Media Supplement (Sigma, I3146) 1 ml, Dexamethasone 40 ng/ml, FBS (Gibco) 10 ml. AML12 were maintained in a humidified atmosphere of 5% CO_2 at 37 °C. Mycoplasma detections were negative in all cells used.

Lentivirus infection and establishment of stable cell lines with overexpression or downregulation of Ptn-dt

Ptn-dt overexpression, interference and the corresponding control lentiviruses were purchased from GenePharma

Company (Shanghai, China), and were named "Oe-NC", "Ptn-dt-Oe", "Sh-NC", "Ptn-dt-Sh-86 (5′−3′sequences: GAACTCTGTAGTACATA-ATAG)", "Ptn-dt-Sh-329 (5′−3′ sequences : CACTAAATAAAGCAGCAATAA)", and "Ptn-dt-Sh-363 (5′−3′ sequences : CTATTGGAGA-GAAATGCATTG)". The full-length cDNA of Ptn-dt was PCR-amplified and subcloned into the lentiviral vector LV5-EF1a-GFP/Puro. The small hairpin RNA (shRNA) of Ptn-dt was subcloned into the lentiviral vector LV3-pGLV-h1-GFP-puro. Hepa1-6, Hepa-1c1c7, and Hepa1-6-luci cells were respectively infected gradiently with over-expression lentiviruses to obtain cell lines with stably overexpressing Ptn-dt and selected with 1.5 μg/ml puro for 2 weeks. To obtain cell lines with stably downregulated Ptn-dt, Hepa1-6, Hepa-1c1c7, and Hepa1-6-luci cells were respectively infected with moderate shRNA and selected at 1.5 μg/ml puro for 2 weeks. The stably expressing cell lines were examined using qRT-PCR. According to the efficiency of overexpression Ptn-dt, Ptn-dt-Oe Clone1 and Ptn-dt-Oe Clone2 were selected for the following experiments. According to the interference efficiency of Ptn-dt, Ptn-dt-Sh-363 (named Ptn-dt- Sh1) and Ptn-dt- Sh-329 (named Ptn-dt- Sh2) were selected for the following experiments.

Colony formation assay

2×10^3 cells counted by cell counter were seeded on each well of a six-well plate and incubated in DMEM with 10% FBS in 5% CO_2 at 37 °C for 14 days. Then, cells were fixed with 4% polyformaldehyde fixed liquid and stained with crystal violet (Beyotime, Shanghai, China) for 30 min and the colonies in the dishes were counted. These experiments were performed in triplicate.

Cells proliferation CCK-8 assay

4×10^3 cells were seeded into each well of 96-well plates and cultured in 100 μl DMEM containing 10% FBS. Before detection, 10 μg/well cell proliferation reagent CCK-8 (Dojindo Laboratories, Kumamoto, Japan) were added, and samples were incubated for additional 2 h at 37 °C and 5% CO_2. Cell growth curves were plotted using the normalized values of OD450, and each point represents the mean of three independent samples. All of the experiments were performed in triplicate.

EdU cell proliferation assay

The assay was performed with EdU kit (RiboBio Co. Ltd, China). The stably expressing cells were grown on coverslips in 12-well plates until they reached about 50% confluency. 50 μM EdU labeling medium was added and incubated cells for additional 2 h at 37 °C. The cells were fixed with 4% formaldehyde for 30 min at room temperature and treated with 0.5% Triton X-100 for 10 min at room temperature. Subsequently, the cells were stained with 1× Apollo® for 20 min. Then, the nuclei of cells were stained with DAPI. At last, the coverslips were mounted by Mowiol (Sigma-Aldrich). The slides were examined with an Olympus BX51 photomicroscope (Olympus, Japan). Five random fields were captured at ×20 magnification for each cell, and Image-Pro Plus software 6.0 (Media Cybernetics, Inc., USA) was used to count the number of EdU-positive cells (identified by Apollo® fluorescence) and total cells (identified by DAPI nuclei staining). The percentage of EdU-positive cells were calculated to demonstrate the proliferation of the cells. Each experiment was repeated independently for three times.

Xenograft tumor model

Subcutaneous tumor growth assays were conducted using male athymic BALB/c nude mice (4−5 weeks old) as previously described [49]. Each mouse was injected with vector-transfected cells (1×10^6) on the left armpit and with control cells (5×10^6) on the right armpit (eight mice per group). The growth of subcutaneous tumors was recorded on days 0, 4, 8, and 12 using the IVIS Lumina II system (Caliper Life Sciences, Hopkinton, MA, USA) each time 10 min after intraperitoneal injection of 4.0 mg of luciferin (Gold Biotech, St Louis, MO, USA) in 50 μl of saline. On day 42, the animals were euthanized, and the tumors were excised, measured, serially sliced and stained with HE and anti-Ki67 antibody. All institutional and national guidelines for the care and use of laboratory animals were followed.

Cell cycle and apoptosis analysis

We performed cell-cycle analysis using the Cell Cycle and Apoptosis Detection Kit (C1052, Beyotime) according to the manufacturer's instructions. FACS was used to analyze the cell-cycle distributions. Cell apoptosis analysis was performed using Annexin V-APC apoptosis analysis kit (Sungene Biotech) according to the manufacturer's instructions. Flow cytometry (Becton Dickinson, San Jose, CA, USA) was used to analyze the ratio of apoptotic cells. Each experiment was repeated independently for three times.

Immunohistochemistry assay

Immunohistochemistry was performed to the target molecules on paraffin sections utilizing a primary antibody against Ki67 (Cell Signaling Technology), and we used 3, 3-diaminobenzidine to visualize the proteins in situ.

RNA pulldown assay and mass spectrometry

Ptn-dt or truncated Ptn-dt and its antisense RNA were in vitro transcribed from vector pSPT19-Ptn-dt, and biotin-labeled with the Biotin RNA Labeling Mix (Roche) and T7 RNA polymerase (Roche), and purified with an RNeasy Mini Kit (Qiagen, Valencia, CA). One milligram of protein from Hepa1-6 cells extracts were incubated with 3 μg of each kind of above-mentioned purified biotinylated transcripts for 1 h at room temperature; complexes were isolated with Dynabeads Myone Streptavidin T1 beads (Invitrogen). The proteins binding to the streptavidin-coupled dynabeads were isolated by sodium dodecyl sulfate-polyacrylamide gel electrophoresis (SDS-PAGE), and then silver-stained. The separated bands in electrophoresis were cut and analyzed by mass spectrometry (ProTech Inc., Norristown, PA).

RNA immunoprecipitation (RIP)

We performed RIP assays using the Magna RIP™ RNA-Binding Protein Immunoprecipitation Kit (Millipore, Bedford, USA) according to the manufacturer's instructions. The HuR antibodies were used for RIP (ab136542). The coprecipitated RNAs were detected using reverse transcription PCR and qRT-PCR. Primer sequences are listed in Supplementary Table S2. Total RNAs (input controls) and isotype controls were performed simultaneously to prove that the detected signals were from RNAs specifically binding to HuR ($n = 3$ for each experiment).

Western blot assay and antibodies

Total cell lysates were prepared in a 1× sodium dodecyl sulfate buffer. Identical quantities of proteins were separated by SDS-PAGE and transferred onto nitrocellulose filter membranes. After incubation with antibodies specific for HuR (Abcam, ab136542), Alk (Abcam, ab16670), Gapdh (Sigma-Aldrich), or beta-actin (Sigma-Aldrich, A5316), the blots were incubated with IRdye 700-conjugated goat anti-mouse IgG and IRdye 800-conjugated goat anti-rabbit IgG and were detected using an Odyssey infrared scanner (Li-Cor). Each experiment was repeated independently for three times.

MicroRNAs production and transient transfection

miR-96 mimics/inhibitor were designed and synthesized by GenePharma Company (Shanghai, China). Transfection was performed with miR-96 mimic/inhibitor and their respective negative control RNAs, using Lipofectamine 3000 kit (Invitrogen, CA) according to the manufacturer's instructions. Cells were harvested 48 h after transfection. The sequences of miR-96 mimics/inhibitor were listed in Supplementary Table S3. LncRNA Ptn-dt transient transfection was performed using Attractene Transfection Reagent (Qiagen, Valencia, CA). Cells were harvested 48 h after transfection.

Prediction of the protein-coding potency of hPTN-DT

We used several tools to predict the protein-coding potency of hPTN-DT, including CPAT [50] (http://lilab.research.bcm.edu/cpat/), CPC [51] (http://cpc.cbi.pku.edu.cn/) and ORF finder (https://www.ncbi.nlm.nih.gov/orffinder/). X inactive specific transcript (XIST) and HOTAIR served as noncoding RNA controls, and ACTB and GAPDH served as coding RNA controls.

Statistical analysis

All data were shown as the mean ± standard deviation. Data analyses and illustration were performed with SPSS Statistics software version 20.0 (IBM Corporation, Armonk, NY) and Prism.v6.01 (GraphPad Software, La Jolla, CA). The assumptions of statistic analysis were tested before performing the analysis. Variance was calculated to make sure proper tests were chosen. For experiments including only two groups, data were evaluated with Student's t test (two-tailed). For experiments including three or more groups, data were analyzed by a one-way analysis of variance. Statistical significance was set at $^{*}P < 0.05$, $^{**}P < 0.01$. $^{***}P < 0.001$. A P value < 0.05 was considered statistically significant.

Acknowledgements We thank Dr. Li Su for the help in flow cytometry technique, and the Institutional Animal Care and Use Committee (the Second Military Medical University, Shanghai, China) for the ethics approval of animal studies. Some elements of Fig. 6 are from LES LABORATOIRES SERVIER. This work was supported by grants from the National Key Basic Research Program (973 project) (2015CB554004) from the Ministry of Science and Technology of China, the National Natural Science Foundation of China (81672775 and 81330037) and the Natural Science Foundation of Shanghai (15XD1504500).

Compliance with ethical standards

Conflict of interest The authors declare that they have no conflict of interest.

References

1. Siegel RL, Miller KD, Jemal A. Cancer statistics, 2016. CA Cancer J Clin. 2016;66:7–30.

2. Venook AP, Papandreou C, Furuse J, de Guevara LL. The incidence and epidemiology of hepatocellular carcinoma: a global and regional perspective. Oncologist. 2010;15(Suppl 4):5–13.
3. Iavarone M, Cabibbo G, Biolato M, Della Corte C, Maida M, Barbara M, et al. Predictors of survival in patients with advanced hepatocellular carcinoma who permanently discontinued sorafenib. Hepatology. 2015;62:784–91.
4. Coulouarn C, Derambure C, Lefebvre G, Daveau R, Hiron M, Scotte M, et al. Global gene repression in hepatocellular carcinoma and fetal liver, and suppression of dudulin-2 mRNA as a possible marker for the cirrhosis-to-tumor transition. J Hepatol. 2005;42:860–9.
5. Liu H, Kho AT, Kohane IS, Sun Y. Predicting survival within the lung cancer histopathological hierarchy using a multi-scale genomic model of development. PLoS Med. 2006;3:e232.
6. Hu M, Shivdasani RA. Overlapping gene expression in fetal mouse intestine development and human colorectal cancer. Cancer Res. 2005;65:8715–22.
7. Yamauchi N, Watanabe A, Hishinuma M, Ohashi K, Midorikawa Y, Morishita Y, et al. The glypican 3 oncofetal protein is a promising diagnostic marker for hepatocellular carcinoma. Mod Pathol. 2005;18:1591–8.
8. Zhang Y, Yang J, Li H, Wu Y, Zhang H, Chen W. Tumor markers CA19-9, CA242 and CEA in the diagnosis of pancreatic cancer: a meta-analysis. Int J Clin Exp Med. 2015;8:11683–91.
9. Becker D, Sfakianakis I, Krupp M, Staib F, Gerhold-Ay A, Victor A, et al. Genetic signatures shared in embryonic liver development and liver cancer define prognostically relevant subgroups in HCC. Mol Cancer. 2012;11:55.
10. Bergstrand CG, Czar B. Demonstration of a new protein fraction in serum from the human fetus. Scand J Clin Lab Invest. 1956;8:174.
11. Yong KJ, Gao C, Lim JS, Yan B, Yang H, Dimitrov T, et al. Oncofetal gene SALL4 in aggressive hepatocellular carcinoma. N Eng J Med. 2013;368:2266–76.
12. Quinn JJ, Chang HY. Unique features of long non-coding RNA biogenesis and function. Nat Rev Genet. 2016;17:47–62.
13. Schmitt AM, Chang HY. Long noncoding RNAs in cancer pathways. Cancer Cell. 2016;29:452–63.
14. Raveh E, Matouk IJ, Gilon M, Hochberg A. The H19 long noncoding RNA in cancer initiation, progression and metastasis—a proposed unifying theory. Mol Cancer. 2015;14:184.
15. Gupta RA, Shah N, Wang KC, Kim J, Horlings HM, Wong DJ, et al. Long non-coding RNA HOTAIR reprograms chromatin state to promote cancer metastasis. Nature. 2010;464:1071–6.
16. Boyerinas B, Park SM, Shomron N, Hedegaard MM, Vinther J, Andersen JS, et al. Identification of let-7-regulated oncofetal genes. Cancer Res. 2008;68:2587–91.
17. Wang F, Yuan JH, Wang SB, Yang F, Yuan SX, Ye C, et al. Oncofetal long noncoding RNA PVT1 promotes proliferation and stem cell-like property of hepatocellular carcinoma cells by stabilizing NOP2. Hepatology. 2014;60:1278–90.
18. Zheng L, Gong W, Liang P, Huang X, You N, Han KQ, et al. Effects of AFP-activated PI3K/Akt signaling pathway on cell proliferation of liver cancer. Tumor Biol. 2014;35:4095–9.
19. Srikantan S, Tominaga K, Gorospe M. Functional interplay between RNA-binding protein HuR and microRNAs. Curr Protein Pept Sci. 2012;13:372–9.
20. Cao C, Sun J, Zhang D, Guo X, Xie L, Li X, et al. The long intergenic noncoding RNA UFC1, a target of MicroRNA 34a, interacts with the mRNA stabilizing protein HuR to increase levels of beta-catenin in HCC cells. Gastroenterology. 2015;148:415–26 e18.
21. Hashiguchi Y, Nishida N, Mimori K, Sudo T, Tanaka F, Shibata K, et al. Down-regulation of miR-125a-3p in human gastric cancer and its clinicopathological significance. Int J Oncol. 2012;40:1477–82.
22. Filipowicz W, Grosshans H. The liver-specific microRNA miR-122: biology and therapeutic potential. Progress Drug Res Fortschr der Arzneim Progres Des Rech Pharm. 2011;67:221–38.
23. Xu F, Zhang X, Lei Y, Liu X, Liu Z, Tong T, et al. Loss of repression of HuR translation by miR-16 may be responsible for the elevation of HuR in human breast carcinoma. J Cell Biochem. 2010;111:727–34.
24. Vishwamitra D, Li Y, Wilson D, Manshouri R, Curry CV, Shi B, et al. MicroRNA 96 is a post-transcriptional suppressor of anaplastic lymphoma kinase expression. Am J Pathol. 2012;180:1772–80.
25. Papadimitriou E, Mikelis C, Lampropoulou E, Koutsioumpa M, Theochari K, Tsirmoula S, et al. Roles of pleiotrophin in tumor growth and angiogenesis. Eur Cytokine Netw. 2009;20:180–90.
26. Powers C, Aigner A, Stoica GE, Mcdonnell K, Wellstein A. Pleiotrophin signaling through anaplastic lymphoma kinase is rate-limiting for glioblastoma growth. J Biol Chem. 2002;277:14153–8.
27. Rosenfield SM, Bowden ET, Cohen-Missner S, Gibby KA, Ory V, Henke RT, et al. Pleiotrophin (PTN) expression and function and in the mouse mammary gland and mammary epithelial cells. PLoS ONE. 2012;7:e47876.
28. Kaur K, Wang X, Fields JK, Johnson DK, Lan L, Pratt M. et al. The fungal natural product azaphilone-9 binds to HuR and inhibits HuR-RNA interaction in vitro. PLoS ONE. 2017;12:e0175471
29. Perezpinera P, Berenson JR, Deuel TF. Pleiotrophin, a multifunctional angiogenic factor: mechanisms and pathways in normal and pathological angiogenesis. Curr Opin Hematol. 2008;15:210–4.
30. Zhang L, Dimberg A. Pleiotrophin is a driver of vascular abnormalization in glioblastoma. Mol Cell Oncol. 2016;3:e1141087.
31. Jemal A, Bray F, Center MM, Ferlay J, Ward E, Forman D. Global cancer statistics. CA Cancer J Clin. 2011;61:69–90.
32. Ma Y, Zhang P, Wang F, Yang J, Yang Z, Qin H. The relationship between early embryo development and tumourigenesis. J Cell Mol Med. 2010;14:2697–701.
33. Kotake Y, Nakagawa T, Kitagawa K, Suzuki S, Liu N, Kitagawa M, et al. Long non-coding RNA ANRIL is required for the PRC2 recruitment to and silencing ofp15(INK4B) tumor suppressor gene. Oncogene. 2011;30:1956–62.
34. Majumdar A, Curley SA, Wu X, Brown P, Hwang JP, Shetty K, et al. Hepatic stem cells and transforming growth factor beta in hepatocellular carcinoma. Nat Rev Gastroenterol Hepatol. 2012;9:530–8.
35. Wang S, Wu X, Liu Y, Yuan J, Yang F, Huang J, et al. Long noncoding RNA H19 inhibits the proliferation of fetal liver cells and the Wnt signaling pathway. FEBS Lett. 2016;590:559–70.
36. Xu D, Yang F, Yuan JH, Zhang L, Bi HS, Zhou CC, et al. Long noncoding RNAs associated with liver regeneration 1 accelerates hepatocyte proliferation during liver regeneration by activating Wnt/β-Catenin signaling. Hepatology. 2013;58:739.
37. Michelotti GA, Tucker A, Swiderska-Syn M, Machado MV, Choi SS, Kruger L, et al. Pleiotrophin regulates the ductular reaction by controlling the migration of cells in liver progenitor niches. Gut. 2016;65:683–92.
38. Park TJ, Jeong BR, Tateno C, Kim HS, Ogawa T, Lim IK, et al. Pleiotrophin inhibits transforming growth factor beta1-induced apoptosis in hepatoma cell lines. Mol Carcinog. 2008;47:784–96.
39. Grzelinski M, Steinberg F, Martens T, Czubayko F, Lamszus K, Aigner A. Enhanced antitumorigenic effects in glioblastoma on double targeting of pleiotrophin and its receptor ALK. Neoplasia. 2009;11:145–56.
40. Koutsioumpa M, Poimenidi E, Pantazaka E, Theodoropoulou C, Skoura A, Megalooikonomou V, et al. Receptor protein tyrosine

phosphatase beta/zeta is a functional binding partner for vascular endothelial growth factor. Mol Cancer. 2015;14:19.
41. Prensner JR, Iyer MK, Balbin OA, Dhanasekaran SM, Cao Q, Brenner JC, et al. Transcriptome sequencing across a prostate cancer cohort identifies PCAT-1, an unannotated lincRNA implicated in disease progression. Nat Biotechnol. 2011;29: 742–9.
42. Martens-Uzunova ES, Bottcher R, Croce CM, Jenster G, Visakorpi T, Calin GA. Long noncoding RNA in prostate, bladder, and kidney cancer. Eur Urol. 2014;65:1140–51.
43. Cooper C, Guo J, Yan Y, Chooniedass-Kothari S, Hube F, Hamedani MK, et al. Increasing the relative expression of endogenous non-coding Steroid Receptor RNA Activator (SRA) in human breast cancer cells using modified oligonucleotides. Nucleic Acids Res. 2009;37:4518–31.
44. Yoon JH, Abdelmohsen K, Srikantan S, Yang X, Martindale JL, De S, et al. LincRNA-p21 suppresses target mRNA translation. Mol Cell. 2012;47:648–55.
45. Wilusz CJ, Wilusz J. HuR and translation—the missing linc (RNA). Mol Cell. 2012;47:495–6.
46. Huang JF, Guo YJ, Zhao CX, Yuan SX, Wang Y, Tang GN, et al. Hepatitis B virus X protein (HBx)-related long noncoding RNA (lncRNA) down-regulated expression by HBx (Dreh) inhibits hepatocellular carcinoma metastasis by targeting the intermediate filament protein vimentin. Hepatology. 2013;57:1882–92.
47. Ulitsky I, Bartel DP. lincRNAs: genomics, evolution, and mechanisms. Cell . 2013;154:26–46.
48. Brennan CM, Steitz JA. HuR and mRNA stability. Cell Mol Life Sci: Cmls. 2001;58:266–77.
49. Yuan JH, Yang F, Wang F, Ma JZ, Guo YJ, Tao QF, et al. A long noncoding RNA activated by TGF-beta promotes the invasion-metastasis cascade in hepatocellular carcinoma. Cancer Cell. 2014;25:666–81.
50. Wang L, Park HJ, Dasari S, Wang S, Kocher J-P, Li W. CPAT: Coding-Potential Assessment Tool using an alignment-free logistic regression model. Nucleic Acids Res. 2013;41:e74–e.
51. Kong L, Zhang Y, Ye Z-Q, Liu X-Q, Zhao S-Q, Wei L, et al. CPC: assess the protein-coding potential of transcripts using sequence features and support vector machine. Nucleic Acids Res. 2007;35(Web Server issue):W345–W9.